A Toolbox for Parameter-Free Predictions of Solid-State Properties of Monodisperse Glassy Polymers with Frozen-In Molecular Orientation

Davide S. A. De Focatiis,[1] C. Paul Buckley[2]

[1]Division of Materials, Mechanics and Structures, University of Nottingham, Nottingham NG7 2RD, United Kingdom

[2]Department of Engineering Science, University of Oxford, Oxford OX1 3PJ, United Kingdom

Correspondence to: D. S. A. De Focatiis (E-mail: davide.defocatiis@nottingham.ac.uk)

Received 1 August 2012; accepted 27 September 2012; published online 31 October 2012
DOI: 10.1002/polb.23196

ABSTRACT: This study presents a toolbox for the prediction of birefringence and craze initiation stress in oriented monodisperse linear amorphous polymers. The toolbox is assembled from a previously proposed melt–solid constitutive model that provides the necessary residual stress components required for predictions of birefringence and craze initiation stress. The Likhtman–McLeish theory for linear rheology of entangled polymers is used to generate the low reduced frequency part of the linear viscoelastic spectrum, the only molar mass-dependent input parameter. All other parameters are obtained by experiment or from literature and can be considered material constants. Toolbox predictions are compared to new experimental data on two grades of linear monodisperse polystyrene (PS) of known molar mass but unknown rheology and to literature data. The toolbox is able to account for the role of molar mass on birefringence and craze initiation stress of PS subjected to supraentanglement orientation processes. © 2012 Wiley Periodicals, Inc. J Polym Sci Part B: Polym Phys 50: 1748–1756, 2012

KEYWORDS: birefringence; constitutive model; crazing; optics; orientation; polystyrene

INTRODUCTION The flow processes that occur during melt processing of polymers can result in varying degrees of frozen-in molecular orientation within polymer products in the solid state. In some classes of products, such as oriented films and fibers, the orientation is intentional and desired. In other classes of products, such as injection moldings and extrusions, it is an unintentional consequence of the competition between processes of shearing and relaxation during the flow of polymer melts. Frozen-in molecular orientation is frequently an important consideration of any design, because its presence leads to anisotropy of many material properties of practical interest. Such anisotropy has been readily observed experimentally through measurable changes of Young's modulus,[1,2] yield stress,[3–6] crazing stress,[7–11] optical birefringence,[1,3,8,12–14] strain-hardening modulus,[4–6,15,16] rate of ageing,[17] and fracture toughness.[18–21]

Most of these properties are not only dependent on the direction of orientation but are also highly sensitive to both the grade of polymer used and to the flow history encountered during processing.[10,14,15] Hence, irrespective of whether the orientation is desired or not, the design of polymeric products generally consists of three interconnected stages: (1) the selection of an appropriate type and grade of polymer; (2) the specification of processing parameters; and (3) the realization of the desired solid-state properties in the processed product. The authors have recently proposed a new, fully three-dimensional constitutive model that uses the linear viscoelastic spectrum in the melt and solid states to predict the nonlinear melt-state and solid-state constitutive response of glassy polymers.[15] By fitting this model to linear viscoelastic rheological data obtained from two monodisperse linear polystyrenes (PS), the authors demonstrated a remarkable result: that it is possible to predict the optical birefringence,[14] the craze initiation stress,[10] and the solid-state mechanical response[15] of a polymer of given molar mass subjected to an arbitrary process history, with a small number of molar mass-independent material constants and experimental measurement of the molar mass-dependent melt-state linear viscoelastic spectrum.

For the special case of linear monodisperse polymers, however, the melt-state linear viscoelastic response can be predicted accurately using the Likhtman and McLeish quantitative physical theory for linear entangled polymer melts.[22] The aim of this article is to take the final step toward completely parameter-free property predictions of solid-state properties of processed polymers. Thus, whereas previously linear rheological experimental data for each polymer grade were used to provide input to the conformational part of the relaxation spectrum, here this is obtained directly from theory. This critical step enables connectivity between theories whose input parameters are all material constants associated with a particular polymer species. The goal is to

enable polymer product designers to make seamless connections between (1) the selected grade of polymer and (2) the defined process history to achieve (3) specific solid-state properties in the processed polymer, by provision of a toolbox of interconnected theories requiring the minimum number of experiments and material constants.

First, new experimental measurements of birefringence and craze initiation stress are carried out on two monodisperse PS grades of significantly different molar mass subjected to a range of uniaxial melt orientation processes. This is followed by an outline of the essential elements of the constitutive model and of the theories for prediction of solid-state properties. Likhtman and McLeish's quantitative linear theory[22] is used to predict the melt-state linear viscoelastic response, and process simulations are performed using parameters computed from this prediction. Outputs from these simulations are used to predict two solid-state properties of practical engineering interest: optical birefringence and craze initiation stress. Toolbox predictions are compared to the new experimental measurements and to literature data and discussed.

EXPERIMENTAL

Materials

The materials used in this study were two samples of monodisperse linear atactic PS with $M_w = 121$ kDa (BE) and $M_w = 966$ kDa (BB) and narrow polydispersities (PDI $= M_w/M_n < 1.1$). Material BE was provided by Prof. Mackley of the University of Cambridge, and material BB was provided by Dr Lian Hutchings, synthesized by living anionic polymerization at the University of Durham. Molar mass measurements were performed relative to PS standards by size exclusion chromatography on a Viscotek TDA 302 machine and an Agilent Technologies PL-GPC 120 with refractive index, viscosity, and light-scattering detectors, and the results are given in Table 1. Previously published experimental data from two further samples of monodisperse linear atactic PS with $M_w = 262$ kDa (AF) and $M_w = 518$ kDa (AG) and narrow polydispersities (PDI $= M_w/M_n < 1.15$) are also used in this study and listed in Table 1.[15]

TABLE 1 Molar Mass Measurements Obtained by Triple Detection SEC for Polystyrene Samples BE and BB used in This Study and for Polystyrene Samples AF and AG from Ref. 15

Code	M_n (kDa)	M_w (kDa)	PDI	Architecture	Source
BE	113.7	121.1	1.07	Linear	This study
BB	900.8	966.4	1.07	Linear	This study
AF	250.9	262.4	1.05	Linear	Ref. 15
AG	449.1	517.6	1.15	Linear	Ref. 15

Production of Oriented Specimens

The need to minimize waste polymer during molding because of limited availability of monodisperse materials, as well as the need to minimize the stress applied to specimens during their removal from the mold, required the development and use of a near net shape molding technique, described in detail elsewhere.[23] Fresh sheets of disposable aluminum foil were used to line the upper and lower surfaces of the molds to provide a repeatable surface texture on the molded specimens. The mold components were lightly sprayed with a dry poly(tetrafluoroethylene) mold release aerosol, before each molding operation. Each cavity of the mold was filled with a small excess of polymer before the mold was placed between preheated press platens. The polymer was held at the molding temperature of 170 °C for a period of 10 min to ensure full relaxation of the polymer, before cooling at a rate of ~15 °C min^{-1}, as described previously,[15] and removal from the mold. With this technique, small numbers of optically isotropic parallelepipedic bars were produced with approximate dimensions of 80 × 6 × 0.5 mm^3.

Oriented specimens were produced by uniaxial melt drawing the prismatic bars of PS in an Instron 5985 testing machine fitted with an environmental chamber, at a range of temperatures T above T_g between 105 and 135 °C. All stretching was carried out at a constant crosshead velocity corresponding to a nominal strain rate of 0.02 s^{-1}, to a fixed stretch ratio of $\lambda = 3$. Specimens were quenched using a cold spray as quickly as possible at the end of the experiment before release. The initial cooling rate was measured on a representative bar as ~15 °C s^{-1}. The oriented bars were unloaded and stored at room temperature before subsequent testing.

Birefringence

Retardation, r, was measured on the central region of all oriented specimens at room temperature using an Olympus BX51-P transmission optical polarizing microscope fitted with strain-free optics, polarizer, and a thick Berek (0–20λ) rotary compensator, under white light, following a previously described procedure.[14] Birefringence, Δn, was computed from measurements of retardation and specimen thickness t as $\Delta n = r/t$. Birefringence values are reported in Figure 1 as a function of draw temperature.

Craze Initiation Stress

A previously described technique was used for the measurement of craze initiation stress of miniature specimens subjected to isochronal 3-point bending creep, and only a brief account is given here.[24] Miniature beams ~6 × 2 × 0.5 mm^3 were cut from the oriented specimens using a custom jig. Specimens were soaked in reagent grade diethylene glycol for 24 h before creep testing. The beams were loaded in 3-point bending creep for 300 s, with the beam axis (and hence the tensile stress) aligned with the direction of orientation, in the presence of diethylene glycol. After unloading, the dimensions of the crazed region were measured using optical microscopy, allowing the determination of the stress σ_c at which crazes have just initiated in the given time (referred to hereafter as the craze initiation stress). Miniature beams were also cut from isotropic molded specimens and subjected to the same creep conditions to determine the isotropic crazing stress σ_c^{iso}. Measurements of the increase in crazing stress with orientation $\sigma_c - \sigma_c^{iso}$ are reported in Figure 2 as a function of draw temperature, as averages

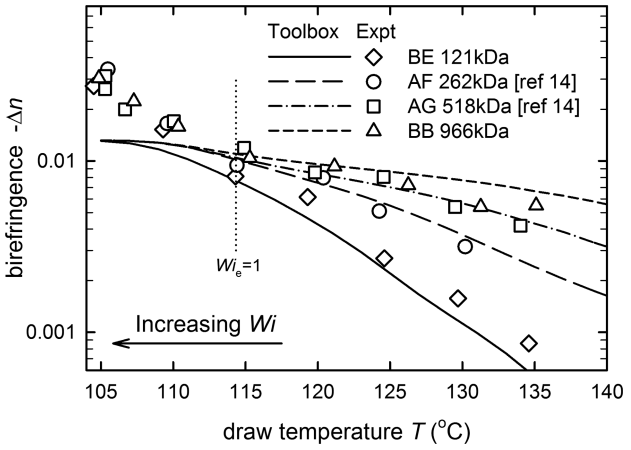

FIGURE 1 Experimental measurements of birefringence as a function of draw temperature for specimens of BE and BB drawn at a strain rate of 0.02 s^{-1} to a draw ratio of $\lambda = 3$ and immediately quenched (triangles and diamonds). Also shown are measurements of birefringence on two further grades of monodisperse polystyrene AF and AG oriented under the same conditions from Ref. 14 (circles and squares). Simulations of birefringence performed using the toolbox and constitutive model (lines).

obtained from a minimum of four beams per experimental condition, and error bars represent two standard errors.

TOOLBOX

The objective of this work is to present a toolbox for the prediction of multiple solid-state properties of glassy polymers with process-induced molecular orientation. A schematic outline of the interdependence between material constants, elements of theory and predictions is provided in Figure 3 to aid the reader.

Melt–Solid Constitutive Model

A fully three-dimensional constitutive model for the melt-state and solid-state response of monodisperse polymer glasses was recently proposed by the present authors, suitable for the prediction of solid-state properties of oriented polymers. The model has been described in detail previously,[15] and only an outline will be given here, with particular focus on the features which render it predictive from a molecular perspective.

The model describes the response of material to a deformation gradient tensor $\mathbf{F}$ in terms of the Cauchy stress tensor $\boldsymbol{\sigma}$, separated into volumetric σ_m and deviatoric $\mathbf{S}$ parts. The volumetric stress is given by $\sigma_m = 1/3 \text{ trace } (\boldsymbol{\sigma}) = K \ln J$, where K is the bulk modulus and $J = \det \mathbf{F}$ is the volumetric part of $\mathbf{F}$. The deviatoric stress $\mathbf{S}$ is expressed as the sum of bond-stretching $\mathbf{S}_b$ and conformational $\mathbf{S}_c$ contributions, $\mathbf{S} = \mathbf{S}_b + \mathbf{S}_c$, from the assumption of additivity of bond-stretching and conformational free energies.

In the bond-stretching part of the model, the deviatoric rate of deformation $\overline{\mathbf{D}} = \frac{1}{2}(\overline{\mathbf{L}} + \overline{\mathbf{L}}^{\mathrm{T}})$ is given by the sum of a linear elastic part and a viscous flow part

$$\mathbf{D} = \frac{\hat{\mathbf{S}}_{b,j}}{2G_b} + \frac{\mathbf{S}_{b,j}}{2G_b\tau_j} \tag{1}$$

for each mode j of a spectrum of Maxwell modes, where $\overline{\mathbf{L}} = \dot{\overline{\mathbf{F}}} \cdot \overline{\mathbf{F}}^{-1}$, $\overline{\mathbf{F}}$ is the deviatoric part of $\mathbf{F}$ and $\dot{\overline{\mathbf{F}}}$ is the time derivative of $\overline{\mathbf{F}}$, $\hat{\mathbf{S}}_j^b$ is the Jaumann rate of stress, G_b is the bond-stretching shear modulus, and τ_j is the glassy relaxation time associated with the jth mode. The deviatoric stress is computed as the sum over all M bond-stretching modes, as $\mathbf{S}_b = \sum_{j=1}^{M} \upsilon_j \mathbf{S}_{b,j}$ where υ_j represents the relative volume fraction of the jth glassy mode. The reader is referred to refs. 25–28 for a more detailed discussion.

The conformational stress is computed from the Rolie–Poly constitutive model,[29] extended for finite extensibility of chains.[15] A conformational stress is computed for each Rolie–Poly mode k across a spectrum of N discrete Rolie–Poly modes by numerical integration of the differential equation describing the evolution of the orientation tensor $\mathbf{T}_k$. The orientation tensor evolves according to

$$\dot{\mathbf{T}}_k = \overline{\mathbf{L}} \cdot \mathbf{T}_k + \mathbf{T}_k \cdot \overline{\mathbf{L}}^{\mathrm{T}} - \frac{1}{\tau_{d,k}}(\mathbf{T}_k - \lambda_k^2\mathbf{I}) - \frac{2}{\tau_{R,k}}\left(\frac{F(\lambda_k)-1}{\lambda_k}\right)\mathbf{T}_k \tag{2}$$

where $\tau_{R,k}$ and $\tau_{d,k}$ are the Rouse and reptation times associated with the kth mode, $\lambda_k = \sqrt{\frac{1}{3}\mathrm{tr}(\mathbf{T}_k)}$ and $F(\lambda_k)$ is a correction factor accounting for finite chain extensibility.[15] The deviatoric conformational stress $\mathbf{S}_{c,k}$ is taken as the deviatoric part of G_e $[\mathbf{T}_k F(\lambda_k)/\lambda_k - \mathbf{I}]$, where G_e is the entanglement modulus. The conformational contribution to the deviatoric stress is thus computed as the sum over all N

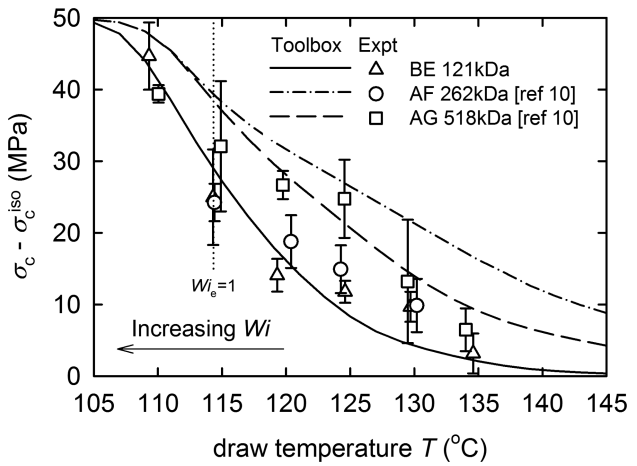

FIGURE 2 Measurements of the increase in craze initiation stress with orientation as a function of draw temperature for specimens of BE drawn at a strain rate of 0.02 s^{-1} to a draw ratio of $\lambda = 3$ and immediately quenched (triangles). Also shown are measurements of craze initiation stress on two further monodisperse polymers drawn under the same conditions from Ref. 10 (circles, squares). Toolbox predictions of the increase in craze initiation stress with orientation performed using the toolbox and constitutive model (lines).

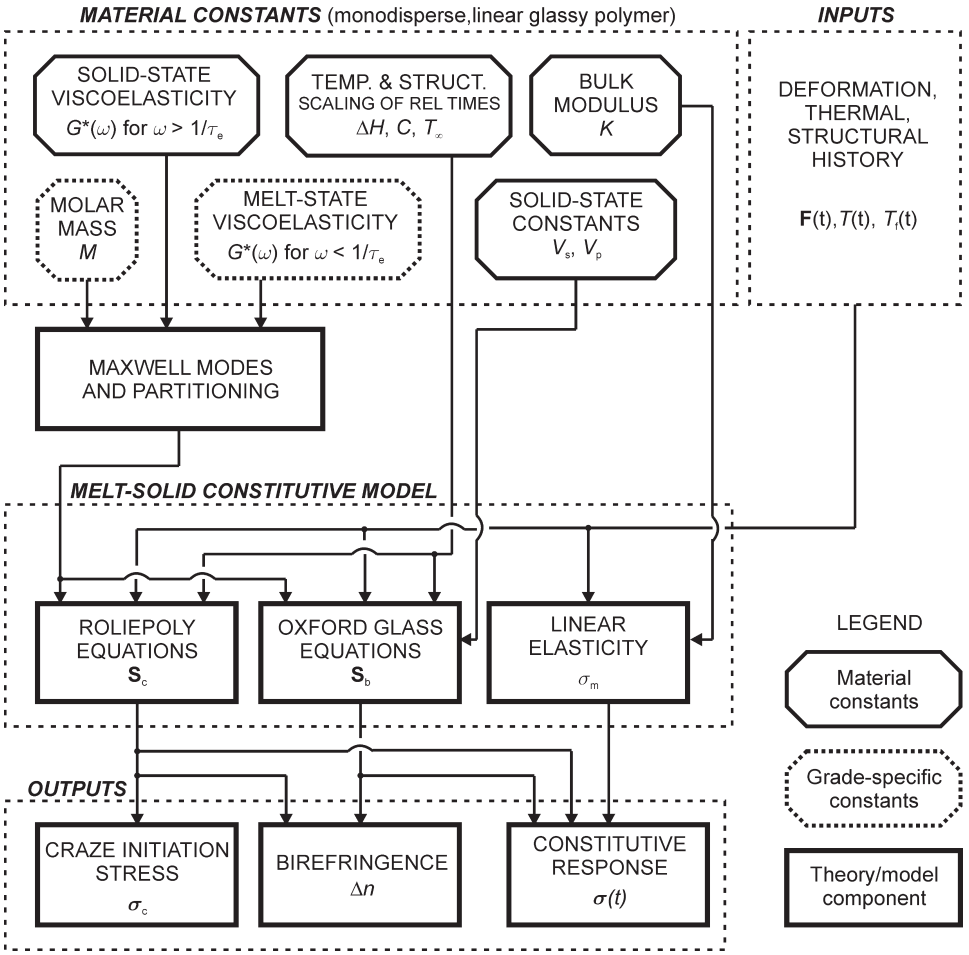

FIGURE 3 A schematic outline of the elements, inputs, and outputs of the toolbox. The process of obtaining Maxwell modes and partitioning is shown in greater detail in Figure 4.

conformational modes, as $\mathbf{S}_c = \sum_{k=1}^{N} \upsilon_k \mathbf{S}_{c,k}$, where υ_k represents the relative volume fraction of the kth Rolie–Poly mode ($\sum_{k=1}^{N} \upsilon_k = 1$).

Model Parameters

Rouse and reptation times are referred back to reference values τ^* at a temperature T^* and structural state T_f^* through shift factors a_T and a_{struct} through $\tau_{R,k} = a_T\, a_{struct}\, \tau^*_{R,k}$ and $\tau_{d,k} = a_T a_{struct}\, \tau^*_{d,k}$. Glassy relaxation times are referred back to reference temperature, structural state, and (unstressed) stress state $\tau^*_{j,0}$ through $\tau_j = a_T a_{struct} a_{\sigma j} \tau^*_{j,0}$. Shift factors obey the following equations:

$$\begin{aligned} a_T &= \exp\left[\frac{\Delta H}{R}\left(\frac{1}{T} - \frac{1}{T^*}\right)\right] \\ a_{struct} &= \exp\left[\frac{C}{T_f - T_\infty} - \frac{C}{T_f^* - T_\infty}\right] \\ a_{\sigma j} &= \frac{V_s \tau^b_{oct,j}}{2RT} \frac{\exp\left(-\frac{V_p \sigma_m}{RT}\right)}{\sinh\left(\frac{V_s \tau^b_{oct,j}}{2RT}\right)} \end{aligned} \tag{3}$$

where $\tau^b_{oct,j}$ is the octahedral shear stress acting on the jth mode, and the rest are material constants: ΔH is the activation enthalpy, T_∞ is the Vogel temperature, C is the Cohen Turnbull constant, and V_s and V_p are the shear and pressure activation volumes. In the simulations that follow, the values of the constants used are obtained from Wu and Buckley[27] and De Focatiis et al.[15] If prediction of the full constitutive response below the glass transition is desired, an evolution equation for fictive temperature with suitable constants can be used, as suggested previously.[26,30] In this work, for simplicity, the polymer is assumed to be in equilibrium for temperatures $T \geq 98.9°C$, and in structural state $T_f = 98.9°C$ for temperatures $T < 98.9°C$, consistent with experimentally measured yield stress measurements.[15]

The material constants G_e, the entanglement modulus, and M_e and τ_e, the mass and Rouse time of one entanglement length, respectively, were identified by treating them as variables for a best fit to the microscopic theory of linear polymer melts of Likhtman and McLeish[31] to linear rheological experimental data on polymers AF and AG.[15] The values of the parameters obtained are: $G_e = 317.9$ kPa, $M_e = 13.14$ kDa, and $\tau_e = 10.57$ s at the reference temperature $T^* = 120°C$, using the optimizer Reptate.[32] The finite extensibility material constant λ_{max} was established as 4.09 from an equivalent Kuhn chain between entanglements.[15] The longest

mode's (whole molecule) Rouse time and reptation time were computed following Collis et al.[33] as

$$\tau^*_{R,1} = Z^2\tau^e$$
$$\tau^*_{d,1} = 3\left(1 - \frac{2.38}{Z^{0.5}} + \frac{4.17}{Z} - \frac{1.55}{Z^{1.5}}\right)Z^3\tau_e \quad (4)$$

where $Z = M/M_e$ represents the number of entanglements.

Viscoelastic Response and Maxwell Modes

Moduli with associated relaxation times for both glassy and conformational modes can be obtained by fitting a discrete spectrum of Maxwell modes to experimental data from viscoelastic experiments, most commonly linear dynamic mechanical analysis (DMA) for glassy modes, and linear melt shear rheology for conformational modes, to cover the range of frequency of interest. In the present authors' original implementation of the constitutive model, the discrete spectrum was fitted to experimental data from two monodisperse linear PS grades.[15] This approach required linear melt rheology to be measured experimentally for each grade of polymer, since, for entangled polymers and for sufficiently low reduced frequencies, this is a strong function of the number of entanglements, and hence of molar mass. It is well known, however, that the high-frequency part of the spectrum generally obtained from DMA data is insensitive to molar mass for sufficiently entangled polymers (as demonstrated by yield stress measurements on several monodisperse PS grades by Wu and Buckley[27]). Hence, a single set of DMA measurements can normally be considered representative of a given polymer species. In principle, only the response at frequencies $\omega < 1/\tau_e$ should be dependent on molar mass because this is the part of the spectrum associated with length scales longer than one entanglement, where Rouse times scale with M^2 and reptation times scale with $M^{3.4}$. In practice, however, this is true only for highly entangled polymers, where the effect of dilution from unentangled ends on relaxation processes is small. From visual observation of experimental rheometric and DMA data on polymers AF and AG, the point at which the response begins to be affected by molar mass was observed to be closer to $\omega \sim 10$ s^{-1} at 120 °C.[15] This compares with $1/\tau_e \approx 0.1$ s^{-1}. Thus, in the toolbox, only the linear viscoelastic response for $\omega \sim 10$ s^{-1} was taken to be a material constant, independent of grade of polymer and used in the evaluation of Maxwell modes that follows. To aid the reader, the process of identification and partitioning of the Maxwell modes is shown schematically in Figure 4.

The linear viscoelastic frequency response can be predicted directly by the quantitative theory of Likhtman and McLeish[31] for a monodisperse polymer of given molar mass, and hence Z, using the material constants G_e, M_e, and τ_e either by appropriate Fourier transformation of the relaxation function[31] or more conveniently by using the optimizer reptate.[32] Figure 5 illustrates theory predictions of the real and imaginary parts of the complex linear viscoelastic modulus for four monodisperse PS grades.

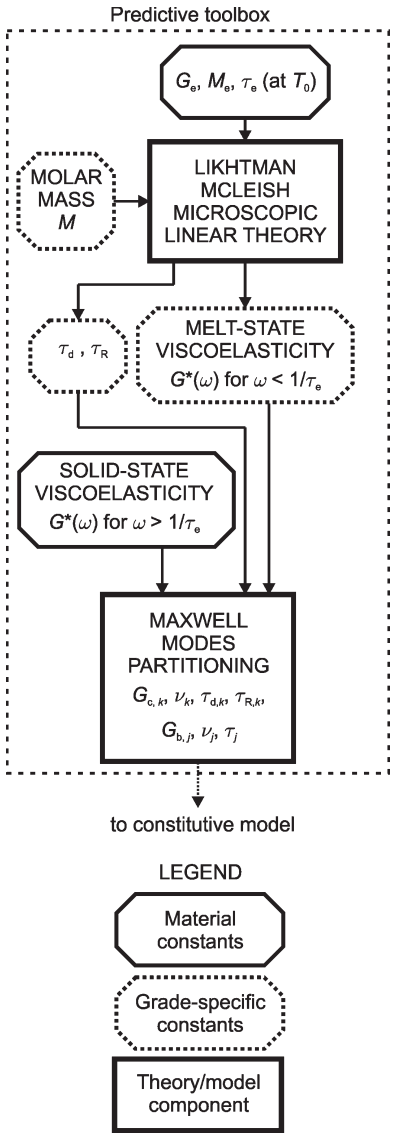

FIGURE 4 The process of obtaining and partitioning discrete Maxwell modes for the constitutive model with the toolbox, using the Likhtman–McLeish theory to generate the linear rheology based on molar mass.

A discrete relaxation spectrum was then fitted to a combination of the experimental linear viscoelastic data for $\omega > 10$ rad s^{-1}, and the linear viscoelastic data from theory predictions for $\omega < 10$ rad s^{-1} (for PS at 120 °C). Starting at the longest relaxation time, $\tau_d = \tau_{d,1}$, one mode was assigned per decade of time to cover the frequency range of interest, using an in-house optimizer minimizing the rms error between the values of log G' and log G'' as obtained from the combination of experimental DMA data and Likhtman–McLeish theory predictions, and as calculated from

$$G' = \sum_{i=1}^{M+N-1} G_i \frac{\omega^2(\tau_{d,i})^2}{1+\omega^2(\tau_{d,i})^2}, \quad G'' = \sum_{i=1}^{M+N-1} G_i \frac{\omega\tau_{d,i}}{1+\omega^2(\tau_{d,i})^2}. \quad (5)$$

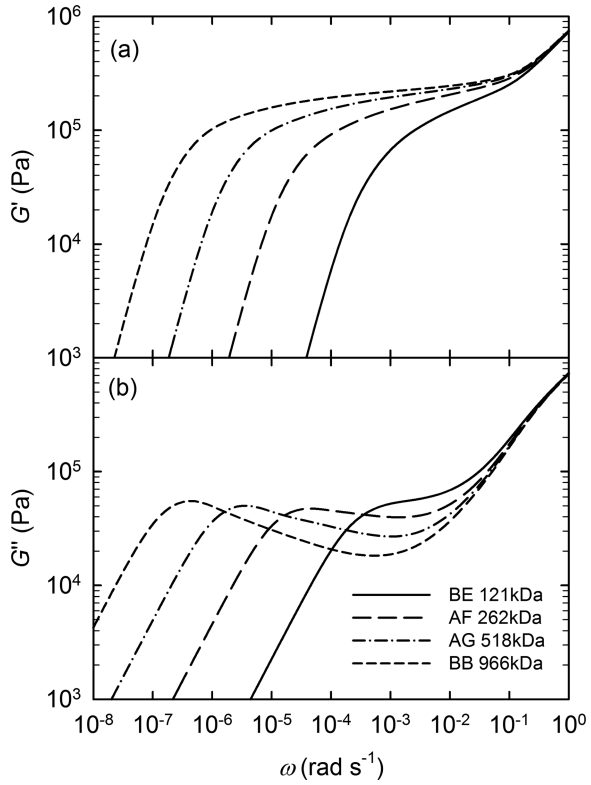

FIGURE 5 Predictions of the (a) storage modulus and (b) loss modulus of four linear monodisperse PS grades using the Likhtman–McLeish linear theory at a reference temperature of 120 °C.

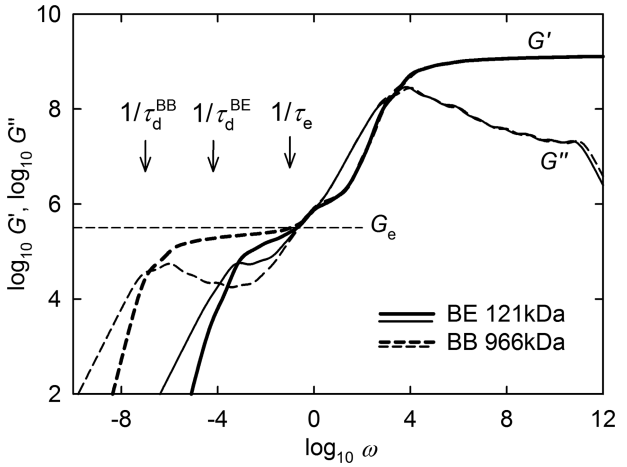

FIGURE 6 Real and imaginary parts of the linear viscoelastic complex shear moduli of materials BE and BB obtained from the Maxwell modes at a reference temperature of 120 °C. Also shown are the positions of the whole molecule reptation times for both polymers, the Rouse time of one entanglement length, and the value of the entanglement modulus G_e.

where M and N are the number of glassy and Rolie–Poly modes, respectively. The condition $\sum_{k=1}^{N} G_k = G_e$ was imposed, restricting Rolie–Poly modes to the conformational response.

The linear viscoelastic complex shear moduli computed from the Maxwell modes for materials BE and BB are illustrated in Figure 6. A total of 5 Rolie–Poly modes and 12 glassy modes were required for material BE, and 7 Rolie–Poly modes and 13 glassy modes for material BB. The volume fractions associated with each mode for materials BE and BB are illustrated in Figure 7. Values of $\tau_{R,k}$ are computed from the equivalent values of Z_k corresponding to each Rolie–Poly mode using eq 4.[15]

Process Simulations

The toolbox is used to generate the necessary parameters (the spectra of Maxwell modes) for the constitutive model to simulate the three stages of the process by which orientation is frozen into the specimens. The first stage consists of an isothermal uniaxial orientation through to $\lambda = 3$ at a rate of $\dot{\varepsilon} = 0.02\ s^{-1}$ for a range of temperatures between 105 and 145 °C, during which time the polymer is assumed to be in structural equilibrium. The second stage consists of a fast quench through to 20 °C at fixed deformation, at a rate of 15 °C s^{-1}. When the temperature falls below 98.9 °C, the specimen is assumed to enter the glassy state, and to remain at a structural state of $T_f = 98.9$ °C for the remainder of the simulation. This structural state is consistent with experimental measurements of yield stress on polymers AF and AG.[15] The third and final stage consists of a fast unloading through to zero net stress at a deformation rate of $\dot{\varepsilon} = -1\ s^{-1}$. Thus, the simulation predicts a state of self-stress for unloaded oriented specimens at room temperature, with non-zero bond-stretching and conformational stress tensors $\mathbf{S}_b = -\mathbf{S}_c$.

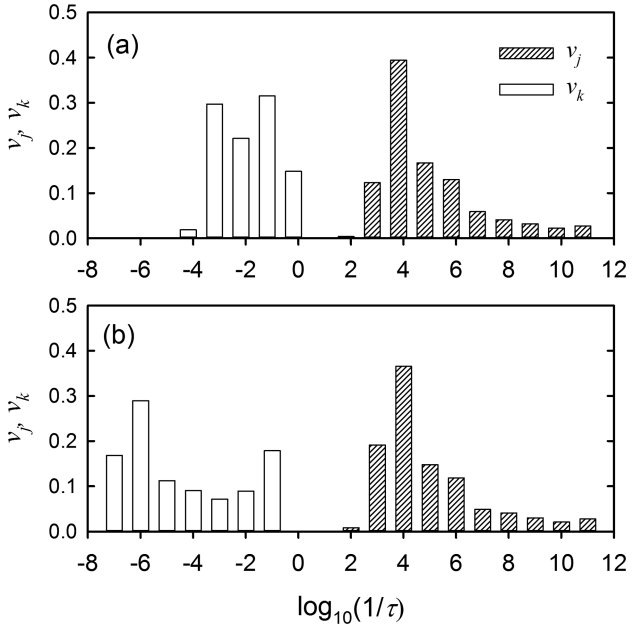

FIGURE 7 Volume fractions of the fitted discrete relaxation spectra obtained (a) for material BE from 17 Maxwell modes (5 Rolie–Poly and 12 glassy) and (b) for material BB from 20 Maxwell modes (7 Rolie–Poly and 13 glassy).

Prediction of Birefringence

In oriented polymers, optical birefringence arises from two independent sources: bond-stretching distortions and conformational alignment of the molecules. Hence, birefringence can be computed as the sum of two independent contributions: one arising from the in-plane principal bond-stretching stress difference ΔS_b and another from the in-plane conformational principal stress difference ΔS_c. In terms of the multimodal constitutive model, this is expressed as

$$\Delta n = \Delta n_b + \Delta n_c = C_b \sum_{j=1}^{M} \upsilon_j \Delta S_{b,j} + C_c \sum_{k=1}^{N} \upsilon_k \Delta S_{c,k} \frac{H(\lambda_k/\lambda_{max})}{H(1/\lambda_{max})} \quad (6)$$

where $H(x) \simeq 1 + x^2/3 + x^4/3$ is a correction factor accounting for the nonlinear relationship between force and end-to-end distance in chains at large extensions,[14] and $C_b = 8.3 \times 10^{-12}$ Pa^{-1} [34] and $C_c = -4.5 \times 10^{-9}$ Pa^{-1} [35] are the stress-optical coefficients for PS. The reader is advised to consult Ref. 14 for a more detailed discussion. Computations of birefringence from toolbox simulations are shown in Figure 1. For all orientations and materials explored here, due to the substantial difference in magnitude between the conformational and the bond-stretching stress-optical coefficients, the conformational component of birefringence accounts for more than 99.7% of the total birefringence.

Prediction of Craze Initiation Stress

In a previous study of crazing in oriented PS, the present authors demonstrated experimentally that the increase in the stress required for craze formation relative to the isotropic, $\sigma_c - \sigma_c^{iso}$ is proportional to optical birefringence for a wide range of orientations.[9] The justification for this proportionality is based on Maestrini and Kramer's postulate, that a back stress acts to increase the stress required for craze formation σ_c relative to the isotropic σ_c^{iso}.[9] Since for moderate levels of birefringence the conformational birefringence is directly proportional to the conformational deviatoric back stress difference through a stress-optical coefficient C_c, the relationship can be expressed as

$$\sigma_c - \sigma_c^{iso} = \Delta S_c/\beta \quad (7)$$

where β is a constant, previously determined by the present authors using birefringence measurements to be 0.059 ± 0.002 for PS.[10] Thus, knowledge of the frozen-in conformational stress tensor $\mathbf{S}_c$ and of the isotropic craze initiation stress enables predictions of craze initiation stress in uniaxially melt-oriented specimens.

An extensive study of isotropic craze initiation stress performed on 14 monodisperse linear polystyrenes concluded that, for 300 s creep in DEG, and for PS of molar mass of 140 kDa and above, the isotropic craze initiation stress $\sigma_c^{iso} \approx 16.1 \pm 1.4$ MPa is invariant of molar mass.[36] This means that for all polymers considered in this study, it can be effectively considered as a material constant.

The increase in crazing stress relative to the isotropic is computed from the conformational stress difference obtained from toolbox simulations using the constitutive model for the full range of experimental orientation temperatures, for polymers BE, AF, and AG, and is shown in Figure 2.

DISCUSSION

As can be seen in Figure 1, the toolbox is successfully able to account for the role of molar mass on birefringence in oriented PS, and correctly predicts the experimental observation that birefringence increases with molar mass at a given draw temperature. Additionally, the toolbox also accounts for another observation: that the relative effect of molar mass is greatest at the highest draw temperatures, and smallest at the lowest draw temperatures.

The numerical values of birefringence obtained from the toolbox are generally in agreement with the experimental data for the draw temperatures $T \geq 115$ °C. This corresponds to the melt-drawing regime for which the entanglement Weissenberg number $Wi_e < 1$; the temperature at which $Wi_e = \dot{\varepsilon}\tau_e = 1$ is 115.7 °C and is marked on Figure 1. The region on the left, where $Wi_e > 1$, represents a drawing regime where subentanglement stretch of the molecules is occurring, and toolbox predictions of birefringence are smaller than experimental measurements suggest. This discrepancy is expected and has been reported previously.[14,15] The reason for its occurrence is that neither Rolie–Poly modes nor glassy modes take any account of contributions arising from subentanglement stretch. In the region on the right, where $Wi_e < 1$, supraentanglement stretch dominates, and there is good quantitative agreement between predictions and experiment; the average difference between toolbox prediction and experiment is 17% and is largest at the smallest birefringence values, where there is greatest experimental uncertainty due to limits on the measurement accuracy of the compensator.

There is a consistent, small overprediction of birefringence for polymer BB, with the highest molar mass. This could be accounted for by a small degree of residual in-plane molecular orientation in the prismatic bars, after molding and before melt drawing. At the molding temperature of 170 °C, the reptation time $\tau_d = 645$ s is of the same order of magnitude as the time for which the polymer was held at temperature after pressing and before cooling. An alternative explanation is that the polymer could have experienced a small degree of degradation during molding, which would lead to a reduction in molar mass, and hence of relaxation times, orientation, and birefringence at a given draw temperature. Although the polymer could be molded at a higher temperature to limit residual orientation, this also increases the likelihood of degradation, and is a common problem with polymers of very high molar mass.

Predictions of craze initiation stress from the toolbox are compared with experiment in Figure 2. The toolbox is successfully able to account for the role of molar mass on craze initiation stress in oriented PS and correctly predicts increasing crazing stress with molar mass for a given draw

temperature. The toolbox predictions also match the experimental observation that the effect of molar mass on craze initiation stress is greatest at intermediate draw temperatures and smallest at the lowest and highest draw temperatures. At the lowest draw temperatures, relaxation times during melt drawing are very long, and molecular orientation occurs with little to no relaxation (and hence independently of molar mass). At very high temperatures, there is almost complete relaxation during melt drawing, and the oriented polymers craze at a similar stress to isotropic polymers of the same molar mass.

Because of the nature and miniaturization of the crazing experiments, there is more uncertainty on the values obtained from experiment compared with birefringence.[10] The numerical values of the predictions are quantitatively in reasonable agreement with the experimental data, with an average difference between toolbox and experiment of 5.8 MPa, or 34% of the matching measured experimental value, across the full range of materials and draw temperatures explored.

Although the constitutive model has to date only been successful in predicting properties of monodisperse linear polymers, the methodology used in the toolbox is more widely applicable. Through the inclusion of theories for the prediction of the linear and nonlinear viscoelastic response of polymers with different architectures (e.g., long-chain branched,[37] dendrimers,[38] or comb polymers) and with different molar mass distribution (e.g., bimodal[39] or multimodal), it will be possible to predict solid-state properties of a much wider range of industrially relevant glassy polymers. Research is presently underway at our Nottingham laboratory to extend the toolbox and the experimental validation to bimodal monodisperse linear blends, and to fully polydisperse linear polymers.

CONCLUSIONS

This study has presented a toolbox for the prediction of birefringence and craze initiation stress in oriented monodisperse linear polymers of known molar mass but unknown rheology. The toolbox relies on a previously proposed melt–solid constitutive model to provide the necessary information required to predict both birefringence and craze initiation. The Likhtman–McLeish theory for linear rheology of entangled polymers was used to generate part of the linear viscoelastic spectrum required by the constitutive model, and all other parameters required (except the molar mass itself) are material constants. The toolbox was applied to four monodisperse linear grades of PS, for two of which the linear rheology is unknown, to generate the molar mass-dependent input parameters to the constitutive model. All other parameters were material constants.

Simulations of the process of melt drawing at a range of temperatures between 105 and 145 °C, quenching and unloading were performed using the constitutive model. Outputs were then combined with existing theories to produce predictions of birefringence and of craze initiation stress. These were compared to new experimental measurements of birefringence and of craze initiation on two grades of linear monodisperse PS of substantially different molar mass and to literature data.

The toolbox predictions were able to account for all observed experimental trends and, in particular, for the effect of molar mass on both birefringence and craze initiation. Birefringence predictions were on average within 17% of experimentally measured quantities for all supraentanglement orientation states and molar masses probed. As subentanglement orientation is not presently featured in the underlying theory, the constitutive model is not able to correctly predict orientation, and hence birefringence for processes where $Wi_e > 1$. Crazing predictions were on average within 34% of experimentally measured quantities for the full range of orientations and polymers explored.

ACKNOWLEDGEMENTS

The authors acknowledge the contributions of Malcolm Mackley of the University of Cambridge, and of Lian Hutchings of the University of Durham in the supply of monodisperse polystyrenes; of the technical staff at the Universities of Nottingham and Oxford for facilitating the orientation experiments; of Shehu Mohammed of the University of Nottingham for carrying out preliminary crazing experiments; and of the Microscale Polymer Processing consortium partners for helpful discussions. This work was supported by Engineering and Physical Sciences Research Council grants GR/T11845/01 and EP/J007978/1.

REFERENCES AND NOTES

1 Biswas, P. K.; Sengupta, S.; Basu, A. N. *Colloid Polym. Sci.* **1988,** *266*, 501–508.

2 Wright, H.; Faraday, C. S. N.; White, E. F. T.; Treloar, L. R. G. *J. Phys. D: Appl. Phys.* **1971,** *4*, 2002–2014.

3 De Francesco, A.; Duckett, R. A. *Polymer* **2004,** *45*, 8005–8011.

4 Arruda, E. M.; Boyce, M. C.; Quintus-Bosz, H. In Plastics and Plastic Composites: Material Properties, Part Performance, and Process Simulation; Stokes, V. K., Ed.; New York, **1991;** MD-Vol. *29*, pp 1–12.

5 Senden, D. J. A.; Van Dommelen, J. A. W.; Govaert, L. E. *J. Polym. Sci. Part B: Polym. Phys.* **2010,** *48*, 1483–1494.

6 Arruda, E. M.; Boyce, M. C. *Int. J. Plast.* **1993,** *9*, 697–720.

7 Beardmore, P.; Rabinwitz, S. *J. Mater. Sci.* **1975,** *10*, 1763–1770.

8 Retting, W. *Colloid Polym. Sci.* **1979,** *257*, 689–710.

9 Maestrini, C.; Kramer, E. J. *Polymer* **1991,** *32*, 609–618.

10 De Focatiis, D. S. A.; Buckley, C. P. *Polymer* **2011,** *52*, 4045–4053.

11 Farrar, N. R.; Kramer, E. J. *Polymer* **1981,** *22*, 691–698.

12 De Francesco, A.; Duckett, R. A. *Polymer* **2004,** *45*, 4297–4306.

13 Bornarel, A. C.; White, J. R. *Polym. Polym. Compos.* **1998,** *6*, 287–294.

14 De Focatiis, D. S. A.; Buckley, C. P. *Macromolecules* **2011,** *44*, 3085–3095.

15 De Focatiis, D. S. A.; Embery, J.; Buckley, C. P. *J. Polym. Sci. Part B: Polym. Phys.* **2010,** *48*, 1449–1463.

16 Hine, P. J.; Duckett, A.; Read, D. J. *Macromolecules* **2007,** *40*, 2782–2790.

17 Shelby, M. D.; Wilkes, G. L. *Polymer* **1998,** *39*, 6767–6779.

18 Gotham, K. V.; Scrutton, I. N. *Polymer* **1978,** *19*, 341–347.

19 Embery, J.; Graham, R. S.; Duckett, R. A.; Groves, D.; Collis, M.; Mackley, M. R.; McLeish, T. C. B. *J. Polym. Sci. Part B: Polym. Phys.* **2007,** *45*, 377–394.

20 Broutman, L. J.; McGarry, F. J. *J. Appl. Polym. Sci.* **1965,** *9*, 609–626.

21 Curtis, J. W. *J. Phys. D: Appl. Phys.* **1970,** *3*, 1413–1422.

22 Likhtman, A. E.; McLeish, T. C. B. *Macromolecules* **2002,** *35*, 6332–6343.

23 De Focatiis, D. S. A. *Polym. Test.* **2012,** *31*, 550–556.

24 De Focatiis, D. S. A.; Buckley, C. P. *Polym. Test.* **2008,** *27*, 136–145.

25 Buckley, C. P.; Jones, D. C. *Polymer* **1995,** *36*, 3301–3312.

26 Buckley, C. P.; Dooling, P. J.; Harding, J.; Ruiz, C. *J. Mech. Phys. Solids* **2004,** *52*, 2355–2377.

27 Wu, J. J.; Buckley, C. P. *J. Polym. Sci. Part B: Polym. Phys.* **2004,** *42*, 2027–2040.

28 Dooling, P. J.; Buckley, C. P.; Rostami, S.; Zahlan, N. *Polymer* **2002,** *43*, 2451–2465.

29 Likhtman, A. E.; Graham, R. S. *J. Non-Newtonian Fluid Mech.* **2003,** *114*, 1–12.

30 Figiel, L.; Dunne, F. P. E.; Buckley, C. P. *Modell. Simul. Mater. Sci. Eng.* **2010,** *18*, 015001 (21pp).

31 Likhtman, A. E.; Milner, S. T.; McLeish, T. C. B. *Phys. Rev. Lett.* **2000,** *85*, 4550–4553.

32 Ramirez, J.; Likhtman, A. E. Rheology of Entangled Polymers: Toolbox for the Analysis of Theory and Experiments (Reptate) **2007,** available at: http://www.reptate.com. Last accessed on 14/4/2009.

33 Collis, M. W.; Lele, A. K.; Mackley, M. R.; Graham, R. S.; Groves, D. J.; Likhtman, A. E.; Nicholson, T. M.; Harlen, O. G.; McLeish, T. C. B.; Hutchings, L. R.; Fernyhough, C. M.; Young, R. N. *J. Rheol.* **2005,** *49*, 501–522.

34 Rudd, J. F.; Andrews, R. D. *J. Appl. Phys.* **1960,** *31*, 818–826.

35 Luap, C.; Karlina, M.; Schweizer, T.; Venerus, D. C. *J. Non-Newtonian Fluid Mech.* **2006,** *138*, 197–203.

36 De Focatiis, D. S. A.; Buckley, C. P.; Hutchings, L. R. *Macromolecules* **2008,** *41*, 4484–4491.

37 McLeish, T. C. B.; Larson, R. G. *J. Rheol.* **1998,** *42*, 81–110.

38 Das, C.; Inkson, N. J.; Read, D. J.; Kelmanson, M. A.; McLeish, T. C. B. *J. Rheol.* **2006,** *50*, 207–235.

39 Auhl, D.; Chambon, P.; McLeish, T. C. B.; Read, D. *J. Phys. Rev. Lett.* **2009,** *103*, 136001 (4pp).